

Scaled momentum distributions for K_S^0 and $\Lambda/\bar{\Lambda}$ in DIS at HERA

ZEUS Collaboration

Abstract

Scaled momentum distributions for the strange hadrons K_S^0 and $\Lambda/\bar{\Lambda}$ were measured in deep inelastic ep scattering with the ZEUS detector at HERA using an integrated luminosity of 330 pb^{-1} . The evolution of these distributions with the photon virtuality, Q^2 , was studied in the kinematic region $10 < Q^2 < 40000 \text{ GeV}^2$ and $0.001 < x < 0.75$, where x is the Bjorken scaling variable. Clear scaling violations are observed. Predictions based on different approaches to fragmentation were compared to the measurements. Leading-logarithm parton-shower Monte Carlo calculations interfaced to the Lund string fragmentation model describe the data reasonably well in the whole range measured. Next-to-leading-order QCD calculations based on fragmentation functions, FFs, extracted from e^+e^- data alone, fail to describe the measurements. The calculations based on FFs extracted from a global analysis including e^+e^- , ep and pp data give an improved description. The measurements presented in this paper have the potential to further constrain the FFs of quarks, anti-quarks and gluons yielding K_S^0 and $\Lambda/\bar{\Lambda}$ strange hadrons.

The ZEUS Collaboration

H. Abramowicz^{45,ah}, I. Abt³⁵, L. Adamczyk¹³, M. Adamus⁵⁴, R. Aggarwal^{7,c}, S. Antonelli⁴, P. Antonioli³, A. Antonov³³, M. Arneodo⁵⁰, V. Aushev^{26,27,z}, Y. Aushev^{27,z,aa}, O. Bachynska¹⁵, A. Bamberger¹⁹, A.N. Barakbaev²⁵, G. Barbagli¹⁷, G. Bari³, F. Barreiro³⁰, N. Bartosik^{27,ab}, D. Bartsch⁵, M. Basile⁴, O. Behnke¹⁵, J. Behr¹⁵, U. Behrens¹⁵, L. Bellagamba³, A. Bertolin³⁹, S. Bhadra⁵⁷, M. Bindi⁴, C. Blohm¹⁵, V. Bokhonov^{26,z}, T. Bołd¹³, K. Bondarenko²⁷, E.G. Boos²⁵, K. Borras¹⁵, D. Boscherini³, D. Bot¹⁵, I. Brock⁵, E. Brownson⁵⁶, R. Brugnera⁴⁰, N. Brümmer³⁷, A. Bruni³, G. Bruni³, B. Brzozowska⁵³, P.J. Bussey²⁰, B. Bylsma³⁷, A. Caldwell³⁵, M. Capua⁸, R. Carlin⁴⁰, C.D. Catterall⁵⁷, S. Chekanov¹, J. Chwastowski^{12,e}, J. Ciborowski^{53,al}, R. Ciesielski^{15,g}, L. Cifarelli⁴, F. Cindolo³, A. Contin⁴, A.M. Cooper-Sarkar³⁸, N. Coppola^{15,h}, M. Corradi³, F. Corriveau³¹, M. Costa⁴⁹, G. D'Agostini⁴³, F. Dal Corso³⁹, J. del Peso³⁰, R.K. Dementiev³⁴, S. De Pasquale^{4,a}, M. Derrick¹, R.C.E. Devenish³⁸, D. Dobur^{19,s}, B.A. Dolgoshein^{33,†}, G. Dolinska^{26,27}, A.T. Doyle²⁰, V. Drugakov¹⁶, L.S. Durkin³⁷, S. Dusini³⁹, Y. Eisenberg⁵⁵, P.F. Ermolov^{34,†}, A. Eskreys^{12,†}, S. Fang^{15,i}, S. Fazio⁸, J. Ferrando³⁸, M.I. Ferrero⁴⁹, J. Figiel¹², M. Forrest^{20,v}, B. Foster^{38,ad}, G. Gach¹³, A. Galas¹², E. Gallo¹⁷, A. Garfagnini⁴⁰, A. Geiser¹⁵, I. Gialas^{21,w}, L.K. Gladilin^{34,ac}, D. Gladkov³³, C. Glasman³⁰, O. Gogota^{26,27}, Yu.A. Golubkov³⁴, P. Göttlicher^{15,j}, I. Grabowska-Bołd¹³, J. Grebenyuk¹⁵, I. Gregor¹⁵, G. Grigorescu³⁶, G. Grzelak⁵³, O. Gueta⁴⁵, M. Guzik¹³, C. Gwenlan^{38,ae}, T. Haas¹⁵, W. Hain¹⁵, R. Hamatsu⁴⁸, J.C. Hart⁴⁴, H. Hartmann⁵, G. Hartner⁵⁷, E. Hilger⁵, D. Hochman⁵⁵, R. Hori⁴⁷, K. Horton^{38,af}, A. Hüttmann¹⁵, Z.A. Ibrahim¹⁰, Y. Iga⁴², R. Ingbir⁴⁵, M. Ishitsuka⁴⁶, H.-P. Jakob⁵, F. Januschek¹⁵, T.W. Jones⁵², M. Jüngst⁵, I. Kadenko²⁷, B. Kahle¹⁵, S. Kananov⁴⁵, T. Kanno⁴⁶, U. Karshon⁵⁵, F. Karstens^{19,t}, I.I. Katkov^{15,k}, M. Kaur⁷, P. Kaur^{7,c}, A. Keramidis³⁶, L.A. Khein³⁴, J.Y. Kim⁹, D. Kisielewska¹³, S. Kitamura^{48,aj}, R. Klanner²², U. Klein^{15,l}, E. Koffeman³⁶, P. Kooijman³⁶, Ie. Korol^{26,27}, I.A. Korzhavina^{34,ac}, A. Kotański^{14,f}, U. Kötz¹⁵, H. Kowalski¹⁵, O. Kuprash¹⁵, M. Kuze⁴⁶, A. Lee³⁷, B.B. Levchenko³⁴, A. Levy⁴⁵, V. Libov¹⁵, S. Limentani⁴⁰, T.Y. Ling³⁷, M. Lisovyi¹⁵, E. Lobodzinska¹⁵, W. Lohmann¹⁶, B. Löhr¹⁵, E. Lohrmann²², K.R. Long²³, A. Longhin³⁹, D. Lontkovskiy¹⁵, O.Yu. Lukina³⁴, J. Maeda^{46,ai}, S. Magill¹, I. Makarenko¹⁵, J. Malka¹⁵, R. Mankel¹⁵, A. Margotti³, G. Marini⁴³, J.F. Martin⁵¹, A. Mastroberardino⁸, M.C.K. Mattingly², I.-A. Melzer-Pellmann¹⁵, S. Mergelmeyer⁵, S. Miglioranzi^{15,m}, F. Mohamad Idris¹⁰, V. Monaco⁴⁹, A. Montanari¹⁵, J.D. Morris^{6,b}, K. Mujkic^{15,n}, B. Musgrave¹, K. Nagano²⁴, T. Namsou^{15,o}, R. Nania³, A. Nigro⁴³, Y. Ning¹¹, T. Nobe⁴⁶, U. Noor⁵⁷, D. Notz¹⁵, R.J. Nowak⁵³, A.E. Nuncio-Quiroz⁵, B.Y. Oh⁴¹, N. Okazaki⁴⁷, K. Oliver³⁸, K. Olkiewicz¹², Yu. Onishchuk²⁷, K. Papageorgiu²¹, A. Parenti¹⁵, E. Paul⁵, J.M. Pawlak⁵³, B. Pawlik¹², P. G. Pelfer¹⁸, A. Pellegrino³⁶, W. Perlański^{53,am}, H. Perrey¹⁵, K. Piotrkowski²⁹, P. Pluciński^{54,an}, N.S. Pokrovskiy²⁵, A. Polini³, A.S. Proskuryakov³⁴, M. Przybycień¹³, A. Raval¹⁵, D.D. Reeder⁵⁶, B. Reisert³⁵, Z. Ren¹¹, J. Repond¹, Y.D. Ri^{48,ak}, A. Robertson³⁸, P. Roloff^{15,m}, I. Rubinsky¹⁵, M. Rusa⁵⁰, R. Sacchi⁴⁹, A. Sali²⁷, U. Samson⁵, G. Sartorelli⁴, A.A. Savin⁵⁶, D.H. Saxon²⁰, M. Schioppa⁸, S. Schlenstedt¹⁶, P. Schleper²², W.B. Schmidke³⁵, U. Schneekloth¹⁵, V. Schönberg⁵, T. Schörner-Sadenius¹⁵, J. Schwartz³¹, F. Sciulli¹¹, L.M. Shcheglova³⁴, R. Shehzadi⁵, S. Shimizu^{47,m}, I. Singh^{7,c}, I.O. Skillicorn²⁰, W. Słomiński¹⁴, W.H. Smith⁵⁶, V. Sola⁴⁹, A. Solano⁴⁹, D. Son²⁸, V. Sosnovtsev³³, A. Spiridonov^{15,p}, H. Stadie²², L. Stanco³⁹, A. Stern⁴⁵, T.P. Stewart⁵¹, A. Stifutkin³³, P. Stopa¹², S. Suchkov³³, G. Susinno⁸, L. Suszycki¹³, J. Sztuk-Dambietz²²,

D. Szuba²², J. Szuba^{15,q}, A.D. Tapper²³, E. Tassi^{8,d}, J. Terrón³⁰, T. Theedt¹⁵, H. Tiecke³⁶, K. Tokushuku^{24,x}, O. Tomalak²⁷, J. Tomaszewska^{15,r}, T. Tsurugai³², M. Turcato²², T. Tymieniecka^{54,ao}, M. Vázquez^{36,m}, A. Verbytskyi¹⁵, O. Viazlo^{26,27}, N.N. Vlasov^{19,u}, O. Volynets²⁷, R. Walczak³⁸, W.A.T. Wan Abdullah¹⁰, J.J. Whitmore^{41,ag}, L. Wiggers³⁶, M. Wing⁵², M. Wlasenko⁵, G. Wolf¹⁵, H. Wolfe⁵⁶, K. Wrona¹⁵, A.G. Yagües-Molina¹⁵, S. Yamada²⁴, Y. Yamazaki^{24,y}, R. Yoshida¹, C. Youngman¹⁵, A.F. Żarnecki⁵³, L. Zawiejski¹², O. Zenaiev¹⁵, W. Zeuner^{15,m}, B.O. Zhautykov²⁵, N. Zhmak^{26,z}, C. Zhou³¹, A. Zichichi⁴, Z. Zolkapli¹⁰, M. Zolko²⁷, D.S. Zotkin³⁴

1 *Argonne National Laboratory, Argonne, Illinois 60439-4815, USA*^A
2 *Andrews University, Berrien Springs, Michigan 49104-0380, USA*
3 *INFN Bologna, Bologna, Italy*^B
4 *University and INFN Bologna, Bologna, Italy*^B
5 *Physikalisches Institut der Universität Bonn, Bonn, Germany*^C
6 *H.H. Wills Physics Laboratory, University of Bristol, Bristol, United Kingdom*^D
7 *Panjab University, Department of Physics, Chandigarh, India*
8 *Calabria University, Physics Department and INFN, Cosenza, Italy*^B
9 *Institute for Universe and Elementary Particles, Chonnam National University,*
10 *Kwangju, South Korea*
11 *Jabatan Fizik, Universiti Malaya, 50603 Kuala Lumpur, Malaysia*^E
12 *Nevis Laboratories, Columbia University, Irvington on Hudson, New York 10027,*
13 *USA*^F
14 *The Henryk Niewodniczanski Institute of Nuclear Physics, Polish Academy of*
15 *Sciences, Krakow, Poland*^G
16 *AGH-University of Science and Technology, Faculty of Physics and Applied Com-*
17 *puter Science, Krakow, Poland*^H
18 *Department of Physics, Jagellonian University, Cracow, Poland*
19 *Deutsches Elektronen-Synchrotron DESY, Hamburg, Germany*
20 *Deutsches Elektronen-Synchrotron DESY, Zeuthen, Germany*
21 *INFN Florence, Florence, Italy*^B
22 *University and INFN Florence, Florence, Italy*^B
23 *Fakultät für Physik der Universität Freiburg i.Br., Freiburg i.Br., Germany*
24 *School of Physics and Astronomy, University of Glasgow, Glasgow, United King-*
25 *dom*^D
26 *Department of Engineering in Management and Finance, Univ. of the Aegean,*
27 *Chios, Greece*
28 *Hamburg University, Institute of Experimental Physics, Hamburg, Germany*^I
29 *Imperial College London, High Energy Nuclear Physics Group, London, United*
30 *Kingdom*^D
31 *Institute of Particle and Nuclear Studies, KEK, Tsukuba, Japan*^J
32 *Institute of Physics and Technology of Ministry of Education and Science of Kaza-*
33 *khstan, Almaty, Kazakhstan*
34 *Institute for Nuclear Research, National Academy of Sciences, Kyiv, Ukraine*
35 *Department of Nuclear Physics, National Taras Shevchenko University of Kyiv,*
36 *Kyiv, Ukraine*
37 *Kyungpook National University, Center for High Energy Physics, Daegu, South Ko-*
38 *rea*^K
39 *Institut de Physique Nucléaire, Université Catholique de Louvain, Louvain-la-Neuve,*
40 *Belgium*^L
41 *Departamento de Física Teórica, Universidad Autónoma de Madrid, Madrid,*
42 *Spain*^M
43 *Department of Physics, McGill University, Montréal, Québec, Canada H3A 2T8*^N
44 *Meiji Gakuin University, Faculty of General Education, Yokohama, Japan*^J

33 *Moscow Engineering Physics Institute, Moscow, Russia*^O
 34 *Moscow State University, Institute of Nuclear Physics, Moscow, Russia*^P
 35 *Max-Planck-Institut für Physik, München, Germany*
 36 *NIKHEF and University of Amsterdam, Amsterdam, Netherlands*^Q
 37 *Physics Department, Ohio State University, Columbus, Ohio 43210, USA*^A
 38 *Department of Physics, University of Oxford, Oxford, United Kingdom*^D
 39 *INFN Padova, Padova, Italy*^B
 40 *Dipartimento di Fisica dell' Università and INFN, Padova, Italy*^B
 41 *Department of Physics, Pennsylvania State University, University Park,*
Pennsylvania 16802, USA^F
 42 *Polytechnic University, Sagamihara, Japan*^J
 43 *Dipartimento di Fisica, Università 'La Sapienza' and INFN, Rome, Italy*^B
 44 *Rutherford Appleton Laboratory, Chilton, Didcot, Oxon, United Kingdom*^D
 45 *Raymond and Beverly Sackler Faculty of Exact Sciences, School of Physics,*
Tel Aviv University, Tel Aviv, Israel^R
 46 *Department of Physics, Tokyo Institute of Technology, Tokyo, Japan*^J
 47 *Department of Physics, University of Tokyo, Tokyo, Japan*^J
 48 *Tokyo Metropolitan University, Department of Physics, Tokyo, Japan*^J
 49 *Università di Torino and INFN, Torino, Italy*^B
 50 *Università del Piemonte Orientale, Novara, and INFN, Torino, Italy*^B
 51 *Department of Physics, University of Toronto, Toronto, Ontario, Canada M5S*
1A7^N
 52 *Physics and Astronomy Department, University College London, London, United*
Kingdom^D
 53 *Faculty of Physics, University of Warsaw, Warsaw, Poland*
 54 *National Centre for Nuclear Research, Warsaw, Poland*
 55 *Department of Particle Physics and Astrophysics, Weizmann Institute, Rehovot,*
Israel
 56 *Department of Physics, University of Wisconsin, Madison, Wisconsin 53706, USA*^A
 57 *Department of Physics, York University, Ontario, Canada M3J 1P3*^N

- A* supported by the US Department of Energy
- B* supported by the Italian National Institute for Nuclear Physics (INFN)
- C* supported by the German Federal Ministry for Education and Research (BMBF),
under contract No. 05 H09PDF
- D* supported by the Science and Technology Facilities Council, UK
- E* supported by an FRGS grant from the Malaysian government
- F* supported by the US National Science Foundation. Any opinion, findings and conclusions or recommendations expressed in this material are those of the authors and do not necessarily reflect the views of the National Science Foundation.
- G* supported by the Polish Ministry of Science and Higher Education as a scientific project No. DPN/N188/DESY/2009
- H* supported by the Polish Ministry of Science and Higher Education and its grants for Scientific Research
- I* supported by the German Federal Ministry for Education and Research (BMBF), under contract No. 05h09GUF, and the SFB 676 of the Deutsche Forschungsgemeinschaft (DFG)
- J* supported by the Japanese Ministry of Education, Culture, Sports, Science and Technology (MEXT) and its grants for Scientific Research
- K* supported by the Korean Ministry of Education and Korea Science and Engineering Foundation
- L* supported by FNRS and its associated funds (IISN and FRIA) and by an Inter-University Attraction Poles Programme subsidised by the Belgian Federal Science Policy Office
- M* supported by the Spanish Ministry of Education and Science through funds provided by CICYT
- N* supported by the Natural Sciences and Engineering Research Council of Canada (NSERC)
- O* partially supported by the German Federal Ministry for Education and Research (BMBF)
- P* supported by RF Presidential grant N 4142.2010.2 for Leading Scientific Schools, by the Russian Ministry of Education and Science through its grant for Scientific Research on High Energy Physics and under contract No.02.740.11.0244
- Q* supported by the Netherlands Foundation for Research on Matter (FOM)
- R* supported by the Israel Science Foundation

- a* now at University of Salerno, Italy
- b* now at Queen Mary University of London, United Kingdom
- c* also funded by Max Planck Institute for Physics, Munich, Germany
- d* also Senior Alexander von Humboldt Research Fellow at Hamburg University, Institute of Experimental Physics, Hamburg, Germany
- e* also at Cracow University of Technology, Faculty of Physics, Mathematics and Applied Computer Science, Poland
- f* supported by the research grant No. 1 P03B 04529 (2005-2008)
- g* now at Rockefeller University, New York, NY 10065, USA
- h* now at DESY group FS-CFEL-1
- i* now at Institute of High Energy Physics, Beijing, China
- j* now at DESY group FEB, Hamburg, Germany
- k* also at Moscow State University, Russia
- l* now at University of Liverpool, United Kingdom
- m* now at CERN, Geneva, Switzerland
- n* also affiliated with Universtiy College London, UK
- o* now at Goldman Sachs, London, UK
- p* also at Institute of Theoretical and Experimental Physics, Moscow, Russia
- q* also at FPACS, AGH-UST, Cracow, Poland
- r* partially supported by Warsaw University, Poland
- s* now at Istituto Nucleare di Fisica Nazionale (INFN), Pisa, Italy
- t* now at Haase Energie Technik AG, Neumünster, Germany
- u* now at Department of Physics, University of Bonn, Germany
- v* now at Biodiversität und Klimaforschungszentrum (BiK-F), Frankfurt, Germany
- w* also affiliated with DESY, Germany
- x* also at University of Tokyo, Japan
- y* now at Kobe University, Japan
- z* supported by DESY, Germany
- † deceased
- aa* member of National Technical University of Ukraine, Kyiv Polytechnic Institute, Kyiv, Ukraine
- ab* member of National University of Kyiv - Mohyla Academy, Kyiv, Ukraine
- ac* partly supported by the Russian Foundation for Basic Research, grant 11-02-91345-DFG_a
- ad* Alexander von Humboldt Professor; also at DESY and University of Oxford
- ae* STFC Advanced Fellow
- af* nee Korcsak-Gorzo
- ag* This material was based on work supported by the National Science Foundation, while working at the Foundation.
- ah* also at Max Planck Institute for Physics, Munich, Germany, External Scientific Member
- ai* now at Tokyo Metropolitan University, Japan
- aj* now at Nihon Institute of Medical Science, Japan

ak now at Osaka University, Osaka, Japan

al also at Łódź University, Poland

am member of Łódź University, Poland

an now at Department of Physics, Stockholm University, Stockholm, Sweden

ao also at Cardinal Stefan Wyszyński University, Warsaw, Poland

1 Introduction

The jet fragmentation and hadronisation processes through which coloured partons become bound in colour-neutral hadrons cannot be described within the framework of perturbative QCD (pQCD). Several approaches have been developed which attempt to build a bridge between the fixed-order partonic cross sections and the observed hadrons. Two of the most successful and widely used approaches are the Lund string model [1] and the fragmentation functions (FFs) [2–6]. The Lund string model, relying on a large number of parameters, is interfaced to leading-logarithm parton-shower Monte Carlo models. The FFs are parameterisations of the hadronisation process within the standard framework of leading-twist collinear QCD factorisation, in a similar way to that of the parton distribution functions (PDFs), and are convoluted with the predicted partonic cross sections.

Extensive studies of the fragmentation properties of the hadronic final state have been performed in e^+e^- [7–19], pp [20–23], $p\bar{p}$ [24] and deep inelastic ep scattering¹ (DIS) [25–33] data and have provided information about the fragmentation and hadronisation processes. The measurements provided tests of pQCD and showed that scaling violations are observed. In addition, the comparison of the measurements in different reactions indicated an approximately universal behaviour of quark fragmentation.

In a previous publication [28], the ZEUS Collaboration presented high-precision measurements of inclusive charged-hadron production. Next-to-leading-order (NLO) QCD calculations, based on different FFs obtained from fits [34–36] to e^+e^- data, from fits [37] to e^+e^- , pp and $p\bar{p}$ data and from fits [38,39] to e^+e^- , pp and ep data, were compared to the measurements. The predictions based on the different FFs are similar and fail to provide a good description of the measurements over the full range of applicability of the calculations. The parameterisations [38,40,41] of the FFs for strange hadrons, such as K_S^0 and Λ , are so far largely unconstrained. The ep data presented in this paper have the potential to constrain these FFs over a wide kinematic range.

In this paper, the scaled momentum distributions for K_S^0 and Λ hadrons² are presented for the first time in DIS. The scaled momentum is defined as $x_p = 2P^{\text{Breit}}/\sqrt{Q^2}$, where P^{Breit} is the particle momentum in the Breit frame and Q^2 is the photon virtuality. The Breit frame [42,43] is the frame in which the exchanged virtual boson is purely space-like, with 3-momentum $\mathbf{q} = (0, 0, -Q)$, providing a maximal separation between the products of the beam fragmentation and the hard interaction. The measurements were performed in the current region of the Breit frame, which is equivalent to one hemisphere in e^+e^- annihilations, as functions of Q^2 and x_p . Next-to-leading-order predictions, based on different FFs, and leading-logarithm parton-shower Monte Carlo calculations, interfaced with the Lund string fragmentation model, were compared to the measurements.

¹ Here and in the following, the term “electron” and the symbol “ e ” denote generically both the electron (e^-) and the positron (e^+), unless otherwise stated.

² Here and in the following, the notation Λ includes both the particle and its antiparticle unless otherwise stated.

2 Theoretical framework

In lowest-order QCD, three processes contribute to the DIS cross section, namely the Born ($V^*q \rightarrow q$, with $V^* = \gamma^*, Z^*$), the boson-gluon-fusion ($V^*g \rightarrow q\bar{q}$) and QCD-Compton-scattering ($V^*q \rightarrow qg$) processes. The cross section for the production of an observed hadron, H , in the final state in DIS can be expressed in QCD, using the factorisation theorem, as

$$\sigma(ep \rightarrow e + H + X) = \sum_{j,j'=q,\bar{q},g} f_{j/p}(x, Q) \otimes \hat{\sigma}_{jj'}(x, Q, z) \otimes F_{H/j'}(z, Q),$$

where the sum runs over all possible initial (final)-state partons j (j'), $f_{j/p}$ are the proton PDFs, which give the probability of finding a parton j with momentum fraction x in the proton, $\hat{\sigma}_{jj'}$ is the partonic cross section, which includes the matrix elements for the three processes mentioned above, and $F_{H/j'}$ are the FFs, which give the probability that a hadron H with momentum fraction z originates from parton j' . The scaled momentum variable x_p is an estimator of z . As for the PDFs, the FFs include contributions from quark, anti-quark and gluon fragmentation. Absolute predictions for the FFs cannot be calculated; however, the dependence of the FFs on the scale Q is calculable in pQCD and governed by renormalisation group equations, similar as for the PDFs.

The range of applicability of the FFs is limited to medium to large values of z , since the assumption of massless hadrons leads to a strong singular behaviour for $z \rightarrow 0$. At small z , finite mass corrections are important. However, the inclusion of small- z mass corrections is not compatible with the factorisation theorem and thus the FFs with mass corrections cannot be used with fixed-order calculations. A possible solution is to introduce *a posteriori* mass-correction factors to take this effect into account [37].

A large improvement in the precision of the ingredients of the calculations has been achieved in the last few years. Matrix elements up to NLO accuracy are available for many processes; for DIS, this corresponds to $\mathcal{O}(\alpha_s^2)$. Parton distribution functions have become increasingly more precise, largely due to the high-precision HERA data. On the other hand, FFs, though increasing in accuracy [34–41], still lack the precision of the proton PDFs.

The data most widely used to extract the FFs comes from e^+e^- annihilations into charged hadrons [7–19]. These data are very precise and the predicted cross sections do not depend on PDFs. However, they do not provide information on how to disentangle quark and anti-quark contributions to the FFs and the gluon fragmentation remains largely unconstrained. In addition, the e^+e^- data have poor statistics at large z , leading to large uncertainties in this region of phase space. Several parameterisations of the FFs exist [34–36].

In the last few years, new one-particle inclusive measurements coming from both pp collisions [20–23] and DIS [44] became available. The inclusion of these data in the extraction of the FFs yields a much more complete picture of the fragmentation process and provides a direct handle on quark, anti-quark and gluon contributions. A global QCD analysis of e^+e^- , pp and DIS data is now available for several hadrons [38,39]. This global FF set agrees with the previous extractions,

based on e^+e^- data alone, in the regions of phase space which are also well constrained by e^+e^- data alone.

3 Experimental set-up

A detailed description of the ZEUS detector can be found elsewhere [45, 46]. A brief outline of the components most relevant for this analysis is given below.

Charged particles were tracked in the central tracking detector (CTD) [47–49], the microvertex detector (MVD) [50] and the straw tube tracker (STT) [51]. The CTD and MVD operated in a magnetic field of 1.43 T provided by a thin superconducting solenoid. The CTD consisted of 72 cylindrical drift-chamber layers, organised in nine superlayers covering the polar-angle³ region $15^\circ < \theta < 164^\circ$.

The MVD silicon tracker consisted of a barrel (BMVD) and a forward (FMVD) section. The BMVD contained three layers and provided polar-angle coverage for tracks from 30° to 150° . The four-layer FMVD extended the polar-angle coverage in the forward region to 7° . After alignment, the single-hit resolution of the MVD was $24 \mu\text{m}$. The transverse distance of closest approach (DCA) to the nominal vertex in XY was measured to have a resolution, averaged over the azimuthal angle, of $(46 \oplus 122/p_T) \mu\text{m}$, with p_T in GeV. The STT covered the polar-angle region $5^\circ < \theta < 25^\circ$. For CTD-MVD tracks that pass through all nine CTD superlayers, the momentum resolution was $\sigma(p_T)/p_T = 0.0029p_T \oplus 0.0081 \oplus 0.0012/p_T$, with p_T in GeV.

The high-resolution uranium–scintillator calorimeter (CAL) [52–55] covered 99.7% of the total solid angle and consisted of three parts: the forward (FCAL), the barrel (BCAL) and the rear (RCAL) calorimeters. Each part was subdivided transversely into towers and longitudinally into one electromagnetic section (EMC) and either one (in RCAL) or two (in BCAL and FCAL) hadronic sections (HAC). The smallest subdivision of the calorimeter was called a cell. Under test-beam conditions, the CAL single-particle relative energy resolutions were $\sigma(E)/E = 0.18/\sqrt{E}$ for electrons and $\sigma(E)/E = 0.35/\sqrt{E}$ for hadrons, with E in GeV.

The energy of the scattered electron was corrected for energy loss in the material between the interaction point and the calorimeter using the small-angle rear tracking detector [56, 57] and the presampler [56, 58].

The luminosity was measured using the Bethe-Heitler reaction $ep \rightarrow e\gamma p$ by the luminosity detector [59–61] which consisted of two independent systems. In the first system, the photons were detected by a lead–scintillator calorimeter placed in the HERA tunnel 107 m from the interaction point in the lepton-beam direction. The second system was a magnetic spectrom-

³ The ZEUS coordinate system is a right-handed Cartesian system, with the Z axis pointing in the proton beam direction, referred to as the “forward direction”, and the X axis pointing towards the centre of HERA. The coordinate origin is at the nominal interaction point.

eter arrangement [62], which measured electron-positron pairs from converted photons. The fractional uncertainty on the measured luminosity was 1.8%.

4 Event selection

The data used in this analysis were collected during the running period 2005–2007, when HERA operated with protons of energy $E_p = 920$ GeV and electrons of energy $E_e = 27.5$ GeV, and correspond to an integrated luminosity of 330 pb^{-1} . The criteria to select DIS events are described below.

A three-level trigger system [46, 63] was used to select events online. It relied on the presence of an energy deposition in the CAL compatible with that of a scattered electron. At the third level, an identified electron [64] with an energy larger than 4 GeV was required.

Offline, the kinematic variables Q^2 , inelasticity, y , and the Bjorken scaling variable, x , as well as the boost vector to the Breit frame were reconstructed using the double-angle (DA) method [65], which uses the angles of the scattered electron and of the hadronic system.

Deep inelastic scattering events were selected by the following requirements:

- $E'_e > 10$ GeV, where E'_e is the scattered-electron energy; this ensures a reconstruction efficiency above 95% and a purity of the scattered electron of $\approx 100\%$;
- $y_e \leq 0.95$, where y_e is the inelasticity estimated from the energy and angle of the scattered electron; this excludes events with spurious electrons in the forward region, which are produced predominantly by photoproduction;
- $y_{\text{JB}} \geq 0.04$, where y_{JB} is the inelasticity estimated using the Jacquet-Blondel method [66]; this rejects events for which the DA method gives a poor reconstruction;
- $35 < \delta < 60$ GeV, where $\delta = \sum (E_i - P_{Z_i})$ and E_i is the energy of the i -th CAL cell, P_{Z_i} is the momentum along the Z axis and the sum runs over all CAL cells; this removes the phase space where photoproduction background and events with initial-state radiation are expected;
- $|Z_{\text{vtx}}| < 50$ cm, where Z_{vtx} is the Z component of the position of the primary vertex; this reduces background from events not originating from ep collisions;
- $|X| > 12$ and $|Y| > 12$ cm, where X and Y are the impact positions of the scattered electron on the RCAL, to avoid the low-acceptance region adjacent to the rear beampipe;
- the analysis was restricted to events with $10 < Q^2 < 40000 \text{ GeV}^2$ and $0.001 < x < 0.75$.

These requirements selected a sample of $2.16 \cdot 10^7$ DIS data events.

5 K_S^0 and Λ selection and reconstruction

The strange hadrons K_S^0 and Λ were identified via the charged-decay channels, $K_S^0 \rightarrow \pi^+\pi^-$ and $\Lambda \rightarrow p\pi^-$ ($\bar{\Lambda} \rightarrow \bar{p}\pi^+$). The candidates were reconstructed using two oppositely charged tracks associated with a displaced secondary vertex. In the case of the K_S^0 , the mass of the pion was assigned to both tracks. For the Λ , the mass of the proton was assigned to the track with the largest momentum, whereas the mass of the pion was assigned to the other track, since the proton always has a larger momentum than the pion for Λ baryons with momentum larger than 0.3 GeV.

All tracks were required to be in the region of high CTD acceptance, $|\eta^{\text{track}}| < 1.75$, where $\eta = -\ln(\tan \theta/2)$ is the pseudorapidity in the laboratory frame and θ is the polar angle with respect to the proton beam direction. The tracks had to pass through at least three CTD superlayers and were required to have transverse momenta $P_T^{\text{track}} > 150$ MeV.

The analysis was restricted to the current region of the Breit frame by boosting the tracks to this frame and requiring $P_Z^{\text{Breit}} < 0$, where P_Z^{Breit} is the longitudinal momentum of the track in the Breit frame. The combined four-vector momentum of the two tracks in the Breit frame, P^{Breit} , was used to reconstruct x_p .

Additional selection criteria, similar to those used in a previous analysis [67], were applied to the selected candidates to maximise the purity of the sample with a minimum loss of statistics. These requirements were:

- $dca < 2$ cm, where dca is the distance of closest approach of the two tracks forming the candidate;
- $\chi^2/dof < 5$ for the χ^2 of the secondary vertex fit;
- $M(e^+e^-) > 60$ MeV, to eliminate background from photon conversion;
- $M(p\pi) > 1121$ MeV ($M(\pi^+\pi^-) < 475$ MeV), to eliminate Λ (K_S^0) background from the K_S^0 (Λ) sample;
- $\theta_{2D} < 0.03$ rad, where θ_{2D} is the collinearity angle in the XY plane between the K_S^0 (Λ)-candidate momentum vector and the vector defined by the interaction point and the K_S^0 (Λ) decay vertex;
- $\theta_{3D} < 0.04$ rad, where θ_{3D} is the collinearity angle between the K_S^0 (Λ)-candidate three-momentum vector and the vector defined by the interaction point and the K_S^0 (Λ) decay vertex;
- $L_{XY} > 0.5$ (1) cm, where L_{XY} is the distance between the K_S^0 (Λ)-candidate decay vertex and the primary vertex in the transverse plane;
- $P_T^{\text{PA}} > (<) 0.11$ GeV, where P_T^{PA} is the projection of the pion momentum onto a plane perpendicular to the K_S^0 (Λ) momentum direction (the Podolanski-Armenteros variable [68]).

Figures 1 and 2 show the dca , θ_{2D} , θ_{3D} and L_{XY} distributions for data and Monte Carlo (see Section 6) for K_S^0 and Λ candidates, respectively. The description of the data by the Monte Carlo simulation is adequate.

Figure 3 shows the $M(\pi^+\pi^-)$ and $M(p\pi)$ distributions after these requirements. A small amount of background is observed. The fit shown in Fig. 3 is for illustration only. The number of K_S^0 (Λ) candidates in each bin of x_p and Q^2 was estimated by counting the entries in the signal region, 472 – 522 (1107.0 – 1124.5) MeV, and subtracting the number of expected background entries. The latter was determined from a linear fit to the sideband regions 403 – 422 and 572 – 597 (1086.0 – 1098.2 and 1133.2 – 1144.4) MeV, also indicated in Fig. 3. There were 806 505 (165 875) K_S^0 (Λ) candidates in the data sample. In the current region of the Breit frame, there were 238 153 K_S^0 and 40 728 Λ candidates. A Monte Carlo study showed that 6% of the selected Λ candidates come from higher-baryon decays.

6 Monte Carlo simulation

Samples of Monte Carlo (MC) events were produced to determine the response of the detector and to correct the data to the hadron level. The MC samples were also used to compute predictions to be compared to the measurements.

The generated events were passed through the GEANT 3.21-based [69] ZEUS detector- and trigger-simulation programs [46]. They were reconstructed and analysed by the same program chain as used for the data. Particles with lifetime longer than $3 \cdot 10^{-11}$ s, such as K_S^0 and Λ , were treated as stable at generator level and their decays were simulated by GEANT.

Neutral current DIS events were generated using the program LEPTO 6.5.1 [70]. Radiative effects were estimated using the HERACLES 4.6.6 [71, 72] program with the DJANGO 1.6 [73, 74] interface to LEPTO. HERACLES includes QED corrections for initial- and final-state radiation, vertex and propagator terms, and two-boson exchange. The QCD cascade was simulated using the colour-dipole model (CDM) [75–78], including the leading-order QCD diagrams as implemented in ARIADNE 4.12 [79, 80] and, alternatively, with the MEPS model of LEPTO. Fragmentation into hadrons was performed using the Lund string model [1], as implemented in JETSET 7.41 [81–84]. The default parameter setting from the DELPHI/EMC [19, 85] tune was used for the hadronisation. The CTEQ5D [86] proton PDFs were used for these simulations.

7 Corrections and systematic uncertainties

The measured scaled momentum distributions were corrected to the hadron level and to the QED Born level. The correction factors were calculated bin-by-bin using the MC samples described in Section 6. The correction factors take into account: (i) the event-selection efficiency for the cuts listed in Section 4, but for the Q^2 and x requirements; (ii) the efficiency to identify the K_S^0 and

Λ decays, as specified in Section 5; (iii) the migrations between bins due to detector resolution, which affects in particular the transformation to the Breit frame; (iv) the relevant branching ratios; and (v) the extrapolation to the full phase space. The factors calculated in the measured (x_p, Q^2) bins varied from 0.05 (0.05) to 0.18 (0.11) for K_S^0 (Λ) candidates, and reached ≈ 0.25 for candidates with momentum in the range 1–1.5 GeV and $-1 < \eta < 1$; the lowest values were found for high Q^2 and x_p values. Bins with an acceptance smaller than 0.05 were not used in the analysis. The QED correction factors were computed using the Monte Carlo samples; they are below 5% for $Q^2 < 100 \text{ GeV}^2$ and increase to a maximum of 20% at the highest values of Q^2 .

The total systematic uncertainties on the scaled momentum distributions are larger than the statistical uncertainties in most bins. The statistical uncertainties themselves vary significantly over the kinematic range. For K_S^0 (Λ), they are at the 1 (4)% level at low Q^2 and between 10 to 90% (20 to 70%) over the x_p range at large Q^2 . Many of the systematic uncertainties were observed to scale with the statistical uncertainty. In the following list, typical values of the uncertainties on the scaled momentum distribution are given separately for K_S^0 and Λ , either as percentages of the statistical uncertainty or as absolute values:

- imperfections in the simulation causing uncertainties on DIS event reconstruction and selection resulted in uncertainties of $^{+40}_{-30}\%$ and $^{+50}_{-40}\%$ of the statistical uncertainties. This was evaluated by modifying the selection cuts within the experimental resolutions. At low Q^2 , the variation of the cut on y_{JB} from 0.04 to 0.07 resulted in large uncertainties exceeding these typical values;
- an uncertainty of -2% in the overall tracking efficiency resulted in absolute uncertainties of $+4\%$ and $+4\%$;
- detector-alignment uncertainties affecting the calculation of the boost vector to the Breit frame resulted in uncertainties of $^{+30}_{-25}\%$ and $^{+20}_{-15}\%$ of the statistical uncertainties. This was evaluated by varying separately the simulated polar angle of the scattered electron and of the hadrons by ± 2 mrad;
- uncertainties on the K_S^0 and Λ selection efficiency resulted in uncertainties of $^{+80}_{-60}\%$ and $^{+60}_{-60}\%$ of the statistical uncertainties. This was evaluated by varying the cuts listed in Section 5: the dominant effects were due to modifications of the cuts on θ_{2D} to 0.015 and 0.06 and θ_{3D} to 0.02 and 0.08;
- assumptions concerning the details of the simulation of the hadronic final state resulted in absolute uncertainties of $^{+4}_{-3}\%$ and $^{+10}_{-15}\%$. At large Q^2 , these uncertainties were larger and exceeded $^{+15}_{-80}\%$ and $^{+50}_{-25}\%$. This was estimated by using MEPS instead of CDM in the calculation of the correction factors;
- background-subtraction uncertainties resulted in absolute uncertainties of $^{+2}_{-2}\%$ and $^{+3}_{-4}\%$. At large Q^2 , the uncertainties exceeded these typical values and were as high as $\pm 35\%$ for both

K_S^0 and Λ . This was evaluated by varying the size of the background window by $\pm 40\%$ and changing the background fit function from first to second order.

The systematic uncertainties were added in quadrature for each bin. The total systematic uncertainty is dominated by the uncertainty in the simulation of the hadronic final state. At low Q^2 , the overall tracking efficiency also contributes significantly. At high Q^2 , the uncertainties related to the K_S^0 and Λ selection are important.

8 NLO QCD calculations

Next-to-leading-order QCD calculations, which combine the full NLO matrix elements with the proton PDFs and FFs as explained in Section 2, were compared to the measurements. For the comparison, the observable x_p is assumed to be equal to the variable z . For each bin in x_p and Q^2 , a prediction was derived by numerical integration over the multiplicities $d^2m(H)/dzdQ^2$, with $m(H)$ the number of H per DIS event. Two sets of calculations based on different parameterisations of the FFs were used. The first set was obtained from fits to e^+e^- data and based on the program CYCLOPS [87], called “AKK+CYCLOPS” [36, 37]. The second set was obtained from a global fit to e^+e^- , pp and ep data, called “DSS” [38]. It was used only for K_S^0 predictions.

The AKK+CYCLOPS calculations were performed using Q as the factorisation and renormalisation scales; the number of active quark flavours was set to $n_f = 5$; the proton PDFs were parameterised using the CTEQ6M sets [88] and Λ_{QCD} was set to 226 MeV. The calculations were done assuming massless particles. Hadron-mass effects [89] for K_S^0 and Λ were included as correction factors [37]. The influence on the shapes of the calculated scaled momentum distributions due to the mass effects is expected at small values of x_p and Q^2 , as explained in Section 2.

In the DSS calculations, the scaled momentum distributions were obtained by convoluting the NLO DSS set of FFs together with the MRST NLO [90] PDFs and appropriate NLO coefficient functions. For these calculations, K_S^0 -mass corrections were not included. The predictions were computed as ratios for each bin, such that a later combination of bins is not possible [91].

The uncertainty from terms beyond NLO was estimated by varying the renormalisation scale by factors 0.5 and 2. The uncertainties from FFs could not be evaluated so far; it is to a certain extent represented by the differences in the predictions of AKK+CYCLOPS and DSS. In addition, it should be noted that the DSS FFs were extracted from data at low Q^2 and that the fits are thus almost unconstrained at high Q^2 [38].

9 Results

Scaled momentum distributions, $(1/N)(n(H)/\Delta x_p)$, with $n(H)$ the number of H (K_S^0 or Λ), N the number of DIS events in a given Q^2 bin and Δx_p the width of the x_p bin, were measured in the current region of the Breit frame. The distributions are presented as functions of Q^2 and x_p in the kinematic region of $10 < Q^2 < 40000 \text{ GeV}^2$ and $0.001 < x < 0.75$.

Figure 4 shows the scaled momentum distributions for K_S^0 as functions of Q^2 in different regions of x_p . The results are also presented in Table 1. The data show clear scaling violation. This behaviour is expected on the basis of the QCD description of the parton evolution with increasing Q : the phase space for soft gluon radiation increases, leading to a rise of the number of soft particles with small x_p .

The predictions from the CDM and MEPS models, based on leading-logarithmic matrix elements plus parton shower and the Lund fragmentation model, as described in Section 6, are compared to the measurements in Fig. 4. They describe the shapes of the distributions fairly well while overestimating the overall production of K_S^0 by 10 to 20%.

The NLO QCD calculations, based on full NLO matrix elements and the fragmentation-function approach described in Sections 2 and 8, are also compared to the measurements in Fig. 4 for $x_p > 0.1$. For $z < 0.1$, the calculations become singular.

The AKK+CYCLOPS calculations, based on FFs extracted from e^+e^- data alone, fail to describe the measurements. These calculations predict a much too high K_S^0 rate but for $x_p > 0.6$. These discrepancies might come from the fact that the FFs used in these predictions have a poorly constrained gluon contribution, which is dominant at low x_p .

The DSS calculations, based on FFs extracted from a global analysis, give a good description of the measurements for $x_p > 0.3$ and $10 < Q^2 < 40000 \text{ GeV}^2$. The prediction for this region of phase space is mainly constrained by pp data, which sufficiently constrain the FFs at high x_p . At lower x_p , the DSS calculations fail to describe the data. This can be explained by the fact that the DSS fit in this region of phase space is mostly unconstrained by the available data. Thus, the measurements presented in this paper will help to improve significantly such global fits in this region of phase space.

Figure 5 and Table 2 show the scaled momentum distributions for K_S^0 as functions of x_p in two regions of Q^2 . The predictions of CDM and MEPS give a good description of the data. In both regions of Q^2 , both NLO calculations predict too-steep spectra. At low Q^2 , this effect is especially pronounced.

Figures 6 and 7 show the scaled momentum distributions for Λ . The results are also presented in Tables 3 and 4. Scaling violations are clearly observed. The predictions of CDM and MEPS give a reasonable description of the measurements, but overestimate the overall Λ rate by $\approx 20\%$. The AKK+CYCLOPS NLO calculations fail to describe the measurements. As seen in Fig. 7, the predicted spectra in x_p are, as in the case of K_S^0 , significantly too steep.

ZEUS has previously published measurements of scaled momentum distributions for inclusive charged particles in DIS [28]. These measurements are dominated by the contribution from charged pions. Figure 8 shows the scaled momentum distributions presented in this paper together with those from the inclusive charged particles analysis in the kinematic region of $0.1 < x_p < 0.4$ as functions of Q^2 . For $Q^2 > 100 \text{ GeV}^2$, all distributions show a plateau. At lower Q^2 , and especially at low x_p , sizeable mass effects are expected. This is clearly visible. For $0.1 < x_p < 0.2$, the value of $(1/N)(n(H)/\Delta x_p)$ drops to 10 (20)% of its maximum value for Λ (K_S^0), while for inclusive charged particles, the $(1/N)(n(H)/\Delta x_p)$ value is still 40% of the plateau value at the lowest Q^2 accessible.

10 Summary and conclusions

Scaled momentum distributions for K_S^0 and Λ hadrons were measured for the first time in ep DIS. The distributions were measured in the Q^2 range from 10 to 40000 GeV^2 and $0.001 < x < 0.75$. Scaling violations were clearly observed for both the K_S^0 and Λ hadrons.

Next-to-leading-order QCD calculations, based on different parameterisations of the FFs, were compared to the measurements. The predictions based on FFs extracted from e^+e^- data alone fail to describe the measurements. Those predictions based on a global analysis which include e^+e^- , pp and ep data give an improved description of the measurements. However, they predict a too high production rate of K_S^0 and Λ hadrons at low x_p and Q^2 . The measurements presented in this paper have the potential to constrain significantly the FFs for the strange hadrons K_S^0 and Λ .

Acknowledgements

We thank the DESY Directorate for their strong support and encouragement. The remarkable achievements of the HERA machine group were essential for the successful completion of this work and are greatly appreciated. We are grateful for the support of the DESY computing and network services. The design, construction and installation of the ZEUS detector have been made possible owing to the ingenuity and effort of many people who are not listed as authors. We would like to thank S. Albino, R. Sassot and collaborators for providing their calculations. Special thanks are due to R. Sassot for very useful discussions.

References

- [1] B. Andersson et al., Phys. Rep. 97 (1983) 31.
- [2] G. Altarelli et al., Nucl. Phys. B 160 (1979) 301.
- [3] W. Furmanski and R. Petronzio, Z. Phys. C 11 (1982) 293.
- [4] P. Nason and B.R. Webber, Nucl. Phys. B 421 (1994) 473.
- [5] J.C. Collins and D.E. Soper, Nucl. Phys. B 193 (1981) 381. Erratum in Nucl. Phys. B 213 (1983) 545.
- [6] J.C. Collins and D.E. Soper, Nucl. Phys. B 194 (1982) 445.
- [7] ALEPH Coll., R. Barate et al., Phys. Rep. 294 (1998) 1.
- [8] ALEPH Coll., A. Heister et al., Eur. Phys. J. C 35 (2004) 457.
- [9] AMY Coll., Y.K. Li et al., Phys. Rev. D 41 (1990) 2675.
- [10] DELPHI Coll., P. Abreu et al., Eur. Phys. J. C 5 (1998) 585.
- [11] DELPHI Coll., P. Abreu et al., Phys. Lett. B 459 (1999) 397.
- [12] DELPHI Coll., P. Abreu et al., Eur. Phys. J. C 18 (2000) 203.
- [13] DELPHI Coll., J. Abdallah et al., Phys. Lett. B 643 (2006) 147.
- [14] L3 Coll., P. Achard et al., Phys. Rep. 399 (2004) 71.
- [15] MARK II Coll., A. Petersen et al., Phys. Rev. D 37 (1988) 1.
- [16] OPAL Coll., G. Alexander et al., Z. Phys. C 72 (1996) 191.
- [17] OPAL Coll., G. Abbiendi et al., Eur. Phys. J. C 16 (2000) 407.
- [18] TASSO Coll., W. Braunschweig et al., Z. Phys. C 47 (1990) 187.
- [19] DELPHI Coll., P. Abreu et al., Phys. Lett. B 311 (1993) 408.
- [20] BRAHMS Coll., I. Arsene et al., Phys. Rev. Lett. 98 (2007) 252001.
- [21] PHENIX Coll., S.S. Adler et al., Phys. Rev. Lett. 91 (2003) 241803.
- [22] STAR Coll., J. Adams et al., Phys. Rev. Lett. 97 (2006) 152302.
- [23] STAR Coll., B.I. Abelev et al., Phys. Rev. C 75 (2007) 064901.
- [24] CDF Coll., D.E. Acosta et al., Phys. Rev. D 72 (2005) 052001.

- [25] ZEUS Coll., M. Derrick et al., *Z. Phys. C* 67 (1995) 93.
- [26] ZEUS Coll., J. Breitweg et al., *Phys. Lett. B* 414 (1997) 428.
- [27] ZEUS Coll., J. Breitweg et al., *Eur. Phys. J. C* 11 (1999) 251.
- [28] ZEUS Coll., H. Abramowicz et al., *JHEP* 1006 (2010) 009.
- [29] H1 Coll., F.D. Aaron et al., *Phys. Lett. B* 654 (2007) 148.
- [30] H1 Coll., S. Aid et al., *Nucl. Phys. B* 445 (1995) 3.
- [31] H1 Coll., C. Adloff et al., *Nucl. Phys. B* 504 (1997) 3.
- [32] H1 Coll., F.D. Aaron et al., *Phys. Lett. B* 681 (2009) 125.
- [33] H1 Coll., F.D. Aaron et al., *Eur. Phys. J. C* 61 (2009) 185.
- [34] S. Kretzer, *Phys. Rev. D* 62 (2000) 054001.
- [35] B.A. Kniehl, G. Kramer and B. Pötter, *Phys. Rev. Lett.* 85 (2000) 5288.
- [36] S. Albino et al., *Phys. Rev. D* 75 (2007) 034018.
- [37] S. Albino, B.A. Kniehl and G. Kramer, *Nucl. Phys. B* 803 (2008) 42.
- [38] D. de Florian, R. Sassot and M. Stratmann, *Phys. Rev. D* 75 (2007) 114010.
- [39] D. de Florian, R. Sassot and M. Stratmann, *Phys. Rev. D* 76 (2007) 074033.
- [40] S. Albino, B.A. Kniehl and G. Kramer, *Nucl. Phys. B* 734 (2006) 50.
- [41] F. Arleo, *Eur. Phys. J. C* 61 (2009) 603.
- [42] R.P. Feynman, *Photon-Hadron Interactions*. Benjamin, New York, (1972).
- [43] K.H. Streng, T.F. Walsh and P.M. Zerwas, *Z. Phys. C* 2 (1979) 237.
- [44] A. Hillenbrand. Ph.D. Thesis, Erlangen University, Report DESY-THESIS-2005-035, 2005 (ISSN 1435-8085).
- [45] ZEUS Coll., M. Derrick et al., *Phys. Lett. B* 293 (1992) 465.
- [46] ZEUS Coll., U. Holm (ed.), *The ZEUS Detector*. Status Report (unpublished), DESY (1993), available on <http://www-zeus.desy.de/bluebook/bluebook.html>.
- [47] N. Harnew et al., *Nucl. Inst. Meth. A* 279 (1989) 290.
- [48] B. Foster et al., *Nucl. Phys. Proc. Suppl. B* 32 (1993) 181.
- [49] B. Foster et al., *Nucl. Inst. Meth. A* 338 (1994) 254.

- [50] A. Polini et al., Nucl. Inst. Meth. A 581 (2007) 656.
- [51] S. Fourletov et al., Nucl. Inst. Meth. A 535 (2004) 191.
- [52] M. Derrick et al., Nucl. Inst. Meth. A 309 (1991) 77.
- [53] A. Andresen et al., Nucl. Inst. Meth. A 309 (1991) 101.
- [54] A. Caldwell et al., Nucl. Inst. Meth. A 321 (1992) 356.
- [55] A. Bernstein et al., Nucl. Inst. Meth. A 336 (1993) 23.
- [56] ZEUS Coll., S. Chekanov et al., Eur. Phys. J. C 21 (2001) 443.
- [57] A. Bamberger et al., Nucl. Inst. Meth. A 401 (1997) 63.
- [58] A. Bamberger et al., Nucl. Inst. Meth. A 382 (1996) 419.
- [59] J. Andruszków et al., Preprint DESY-92-066, DESY, 1992.
- [60] ZEUS Coll., M. Derrick et al., Z. Phys. C 63 (1994) 391.
- [61] J. Andruszków et al., Acta Phys. Pol. B 32 (2001) 2025.
- [62] M. Helbich et al., Nucl. Inst. Meth. A 565 (2006) 572.
- [63] W.H. Smith, K. Tokushuku and L.W. Wiggers, *Proc. Computing in High-Energy Physics (CHEP), Annecy, France, Sept. 1992*, C. Verkerk and W. Wojcik (eds.), p. 222. CERN, Geneva, Switzerland (1992). Also in preprint DESY 92-150B.
- [64] H. Abramowicz, A. Caldwell and R. Sinkus, Nucl. Inst. Meth. A 365 (1995) 508.
- [65] S. Bentvelsen, J. Engelen and P. Kooijman, *Proc. of the Workshop on Physics at HERA*, W. Buchmüller and G. Ingelman (eds.), Vol. 1, p. 23. Hamburg, Germany, DESY (1992).
- [66] F. Jacquet and A. Blondel, *Proc. of the Study for an ep Facility for Europe*, U. Amaldi (ed.), p. 391. Hamburg, Germany (1979). Also in preprint DESY 79/48.
- [67] ZEUS Coll., S. Chekanov et al., Phys. Lett. B 652 (2007) 1.
- [68] J. Podolanski and R. Armenteros, Phil. Mag. 43 (1954) 13.
- [69] R. Brun et al., GEANT3, Technical Report CERN-DD/EE/84-1, CERN, 1987.
- [70] G. Ingelman, A. Edin and J. Rathsmann, Comp. Phys. Comm. 101 (1997) 108.
- [71] A. Kwiatkowski, H. Spiesberger and H.-J. Möhring, Comp. Phys. Comm. 69 (1992) 155.
- [72] H. Spiesberger, *An Event Generator for ep Interactions at HERA Including Radiative Processes (Version 4.6)*, 1996, available on <http://www.desy.de/~hspiesb/heracles.html>.

- [73] K. Charchuła, G.A. Schuler and H. Spiesberger, *Comp. Phys. Comm.* 81 (1994) 381.
- [74] H. Spiesberger, *HERACLES and DJANGO: Event Generation for ep Interactions at HERA Including Radiative Processes*, 1998, available on <http://wwwthep.physik.uni-mainz.de/~hspiesb/djangoh/djangoh.html>.
- [75] Y. Azimov et al., *Phys. Lett. B* 165 (1985) 147.
- [76] G. Gustafson, *Phys. Lett. B* 175 (1986) 453.
- [77] G. Gustafson and U. Pettersson, *Nucl. Phys. B* 306 (1988) 746.
- [78] B. Andersson et al., *Z. Phys. C* 43 (1989) 625.
- [79] L. Lönnblad, *Comp. Phys. Comm.* 71 (1992) 15.
- [80] L. Lönnblad, *Z. Phys. C* 65 (1995) 285.
- [81] T. Sjöstrand, *Comp. Phys. Comm.* 82 (1994) 74.
- [82] T. Sjöstrand et al., *Comp. Phys. Comm.* 135 (2001) 238.
- [83] T. Sjöstrand, *Comp. Phys. Comm.* 39 (1986) 347.
- [84] T. Sjöstrand and M. Bengtsson, *Comp. Phys. Comm.* 43 (1987) 367.
- [85] EMC Coll., M. Arneodo et al., *Z. Phys. C* 35 (1987) 417.
- [86] H.L. Lai et al., *Eur. Phys. J. C* 12 (2000) 375.
- [87] D. Graudenz, *Phys. Lett. B* 406 (1997) 178.
- [88] J. Pumplin et al., *JHEP* 0207 (2002) 012.
- [89] S. Albino et al., *Phys. Rev. Lett.* 95 (2005) 232002.
- [90] A.D. Martin et al., *Phys. Lett. B* 531 (2002) 216.
- [91] R. Sassot, private communication.

Q^2 (GeV ²)	$0.0 < x_p < 0.1$	$0.1 < x_p < 0.2$	$0.2 < x_p < 0.3$
10 - 40	$0.031 \pm 0.001^{+0.002}_{-0.001}$	$0.125 \pm 0.001^{+0.008}_{-0.003}$	$0.144 \pm 0.001^{+0.009}_{-0.013}$
40 - 160	$0.171 \pm 0.002^{+0.009}_{-0.006}$	$0.392 \pm 0.003^{+0.018}_{-0.010}$	$0.283 \pm 0.002^{+0.013}_{-0.006}$
160 - 640	$0.551 \pm 0.010^{+0.025}_{-0.018}$	$0.612 \pm 0.010^{+0.028}_{-0.017}$	$0.306 \pm 0.007^{+0.014}_{-0.009}$
640 - 2560	$1.141 \pm 0.038^{+0.087}_{-0.037}$	$0.618 \pm 0.030^{+0.1130}_{-0.016}$	$0.309 \pm 0.029^{+0.047}_{-0.011}$
2560 - 10240	$1.878 \pm 0.168^{+0.095}_{-0.147}$	$0.834 \pm 0.217^{+0.065}_{-0.278}$	$0.115 \pm 0.062^{+0.066}_{-0.054}$
Q^2 (GeV ²)	$0.3 < x_p < 0.4$	$0.4 < x_p < 0.6$	$0.6 < x_p < 1.0$
10 - 40	$0.1112 \pm 0.0008^{+0.0074}_{-0.0130}$	$0.0130 \pm 0.0004^{+0.0041}_{-0.0013}$	$0.0132 \pm 0.0001^{+0.0007}_{-0.0004}$
40 - 160	$0.1571 \pm 0.0019^{+0.0082}_{-0.0033}$	$0.0671 \pm 0.0009^{+0.0038}_{-0.0014}$	$0.0109 \pm 0.0003^{+0.0006}_{-0.0002}$
160 - 640	$0.1585 \pm 0.0060^{+0.0118}_{-0.0051}$	$0.0548 \pm 0.0027^{+0.0050}_{-0.0014}$	$0.0073 \pm 0.0008^{+0.0005}_{-0.0011}$
640 - 2560	$0.1053 \pm 0.0217^{+0.0319}_{-0.0214}$	$0.0558 \pm 0.0141^{+0.0176}_{-0.0028}$	$0.0029 \pm 0.0022^{+0.0014}_{-0.0030}$

Table 1: The measured scaled momentum distributions $(1/N)(n(K_S^0)/\Delta x_p)$ as functions of Q^2 in different regions of x_p . The statistical and systematic uncertainties are also shown.

x_p	$10 < Q^2 < 100 \text{ GeV}^2$	$100 < Q^2 < 40000 \text{ GeV}^2$
0.0 - 0.1	$0.0488 \pm 0.0006^{+0.0024}_{-0.0012}$	$0.4841 \pm 0.0063^{+0.0233}_{-0.0117}$
0.1 - 0.2	$0.1618 \pm 0.0009^{+0.0094}_{-0.0041}$	$0.5740 \pm 0.0061^{+0.0263}_{-0.0132}$
0.2 - 0.3	$0.1648 \pm 0.0009^{+0.0098}_{-0.0035}$	$0.3140 \pm 0.0048^{+0.0142}_{-0.0082}$
0.3 - 0.4	$0.1183 \pm 0.0007^{+0.0077}_{-0.0026}$	$0.1588 \pm 0.0037^{+0.01213}_{-0.0045}$
0.4 - 0.5	$0.0751 \pm 0.0006^{+0.0055}_{-0.0015}$	$0.0760 \pm 0.0027^{+0.0073}_{-0.0017}$
0.5 - 0.6	$0.0452 \pm 0.0004^{+0.0031}_{-0.0010}$	$0.0408 \pm 0.0022^{+0.0037}_{-0.0011}$
0.6 - 0.7	$0.0260 \pm 0.0003^{+0.0017}_{-0.0006}$	$0.0182 \pm 0.0015^{+0.0011}_{-0.0009}$
0.7 - 0.8	$0.0150 \pm 0.0002^{+0.0009}_{-0.0003}$	$0.0101 \pm 0.0012^{+0.0008}_{-0.0016}$
0.8 - 0.9	$0.0073 \pm 0.0001^{+0.0005}_{-0.0003}$	$0.0034 \pm 0.0007^{+0.0007}_{-0.0001}$
0.9 - 1.0	$0.0032 \pm 0.0001^{+0.0002}_{-0.0006}$	$0.0020 \pm 0.0006^{+0.0008}_{-0.0001}$

Table 2: The measured scaled momentum distributions $(1/N)(n(K_S^0)/\Delta x_p)$ as functions of x_p in different regions of Q^2 . Other details as in the caption to Table 1.

Q^2 (GeV ²)	$0.0 < x_p < 0.1$	$0.1 < x_p < 0.2$	$0.2 < x_p < 0.3$
10 - 40	$0.0025 \pm 0.0002^{+0.0003}_{-0.0002}$	$0.0122 \pm 0.0004^{+0.0010}_{-0.0008}$	$0.0189 \pm 0.0005^{+0.0015}_{-0.0014}$
40 - 160	$0.0189 \pm 0.0014^{+0.0012}_{-0.0007}$	$0.0650 \pm 0.0021^{+0.0030}_{-0.0039}$	$0.0656 \pm 0.0018^{+0.0037}_{-0.0036}$
160 - 640	$0.0995 \pm 0.0095^{+0.0085}_{-0.0073}$	$0.1666 \pm 0.0099^{+0.0091}_{-0.0163}$	$0.0960 \pm 0.0066^{+0.0074}_{-0.0038}$
640 - 2560	$0.2313 \pm 0.0427^{+0.0593}_{-0.0567}$	$0.1966 \pm 0.0414^{+0.0124}_{-0.0303}$	$0.1038 \pm 0.0346^{+0.0132}_{-0.0090}$
2560 - 10240	$0.7416 \pm 0.4386^{+0.0577}_{-0.3574}$	$0.1962 \pm 0.1268^{+0.0393}_{-0.1395}$	
Q^2 (GeV ²)	$0.3 < x_p < 0.4$	$0.4 < x_p < 0.6$	$0.6 < x_p < 1.0$
10 - 40	$0.0184 \pm 0.0004^{+0.0011}_{-0.0013}$	$0.0106 \pm 0.0002^{+0.0006}_{-0.0004}$	$0.0021 \pm 0.0001^{+0.0001}_{-0.0001}$
40 - 160	$0.0453 \pm 0.0015^{+0.0028}_{-0.0031}$	$0.0198 \pm 0.0007^{+0.0011}_{-0.0010}$	$0.0020 \pm 0.0002^{+0.0003}_{-0.0001}$
160 - 640	$0.0641 \pm 0.0074^{+0.0034}_{-0.0149}$	$0.0139 \pm 0.0025^{+0.0089}_{-0.0031}$	$0.0041 \pm 0.0009^{+0.0003}_{-0.0008}$
640 - 2560	$0.0653 \pm 0.0436^{+0.0119}_{-0.0244}$		

Table 3: The measured scaled momentum distributions $(1/N)(n(\Lambda)/\Delta x_p)$ as functions of Q^2 in different regions of x_p . Other details as in the caption to Table. 1.

x_p	$10 < Q^2 < 100 \text{ GeV}^2$	$100 < Q^2 < 40000 \text{ GeV}^2$
0.0 - 0.1	$0.00437 \pm 0.00034^{+0.00046}_{-0.00017}$	$0.08307 \pm 0.00638^{+0.00626}_{-0.00826}$
0.1 - 0.2	$0.01822 \pm 0.00059^{+0.00106}_{-0.00109}$	$0.13904 \pm 0.00466^{+0.00677}_{-0.01515}$
0.2 - 0.3	$0.02456 \pm 0.00059^{+0.00163}_{-0.00118}$	$0.09489 \pm 0.00275^{+0.00541}_{-0.00646}$
0.3 - 0.4	$0.02173 \pm 0.00049^{+0.00109}_{-0.00138}$	$0.056013 \pm 0.00188^{+0.00323}_{-0.00353}$
0.4 - 0.5	$0.01387 \pm 0.00035^{+0.00088}_{-0.00030}$	$0.02950 \pm 0.00135^{+0.00181}_{-0.00310}$
0.5 - 0.6	$0.00913 \pm 0.00026^{+0.00054}_{-0.00043}$	$0.014640 \pm 0.00095^{+0.00091}_{-0.00048}$
0.6 - 0.7	$0.00483 \pm 0.00018^{+0.00028}_{-0.00027}$	$0.00534 \pm 0.00051^{+0.00068}_{-0.00034}$
0.7 - 0.8	$0.00245 \pm 0.00011^{+0.00015}_{-0.00024}$	$0.00178 \pm 0.00028^{+0.00032}_{-0.00049}$
0.8 - 0.9	$0.00096 \pm 0.00006^{+0.0011}_{-0.00009}$	$0.00056 \pm 0.00019^{+0.00006}_{-0.00018}$
0.9 - 1.0	$0.00038 \pm 0.00004^{+0.00003}_{-0.00013}$	$0.00032 \pm 0.00013^{+0.00009}_{-0.00023}$

Table 4: *The measured scaled momentum distributions $(1/N)(n(\Lambda)/\Delta x_p)$ as functions of x_p in different regions of Q^2 . Other details as in the caption to Table. 1.*

ZEUS

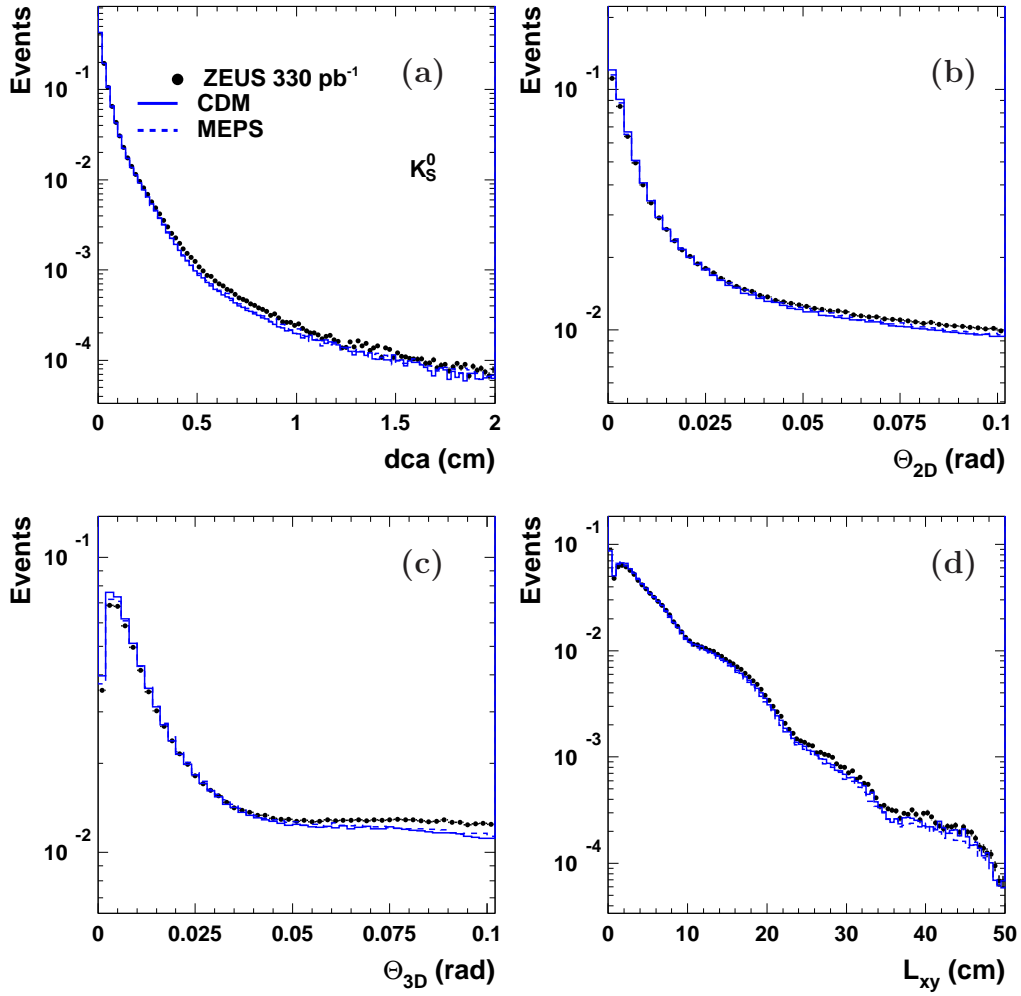


Figure 1: The normalised (a) dca , (b) θ_{2D} , (c) θ_{3D} and (d) L_{XY} distributions for data (dots) and Monte Carlo (histograms) for K_S^0 candidates.

ZEUS

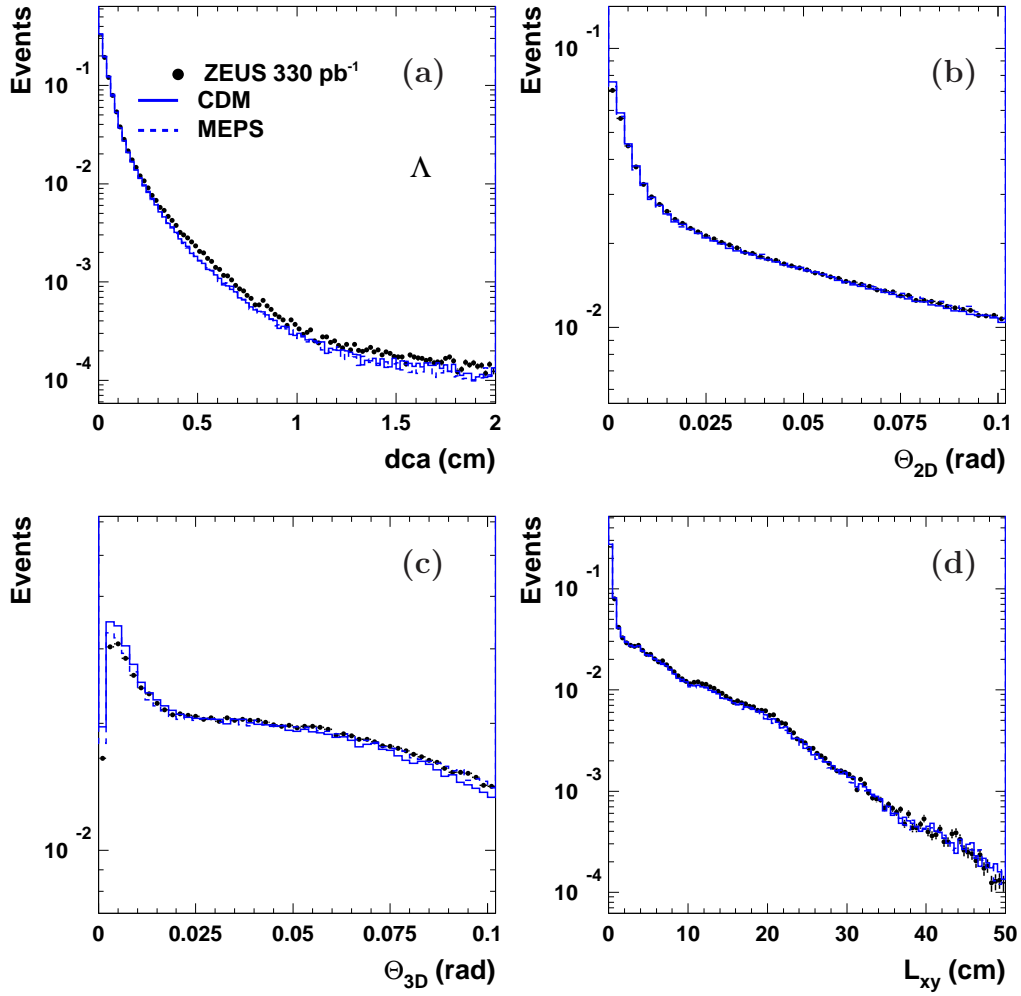


Figure 2: *The normalised (a) dca , (b) θ_{2D} , (c) θ_{3D} and (d) L_{XY} distributions for data (dots) and Monte Carlo (histograms) for Λ candidates.*

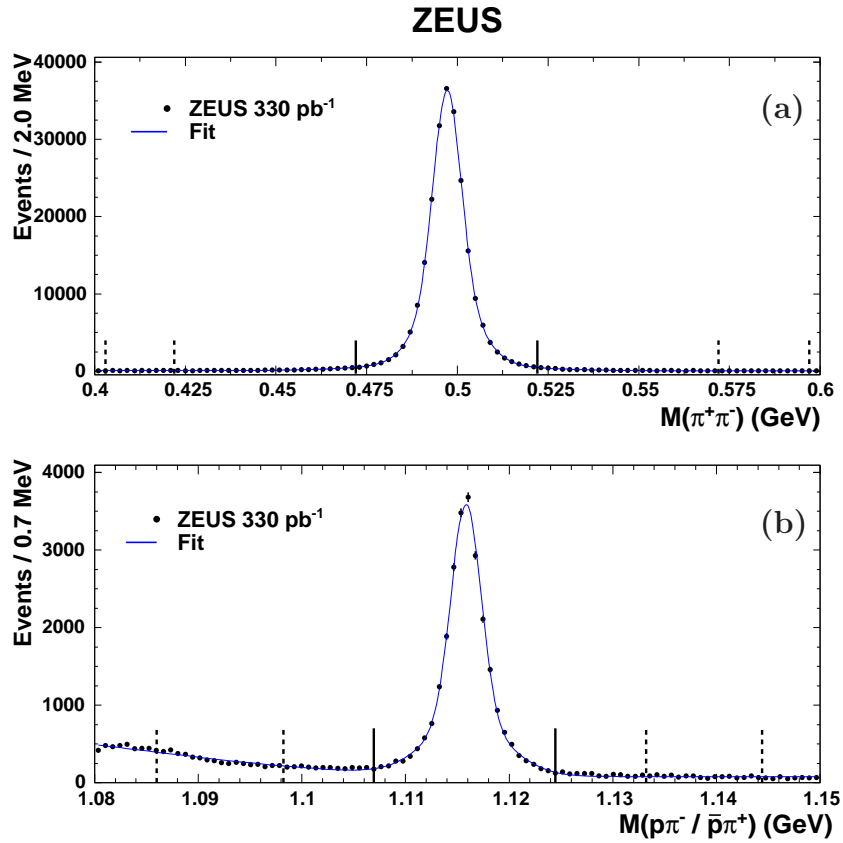


Figure 3: (a) The $\pi^+\pi^-$ invariant-mass distribution for K_S^0 candidates (dots). (b) The $p\pi^-/\bar{p}\pi^+$ invariant-mass distribution for $\Lambda/\bar{\Lambda}$ candidates (dots). In both (a) and (b), the solid line represents an indicative fit by two Gaussians and a (a) linear and (b) quadratic background function. The solid vertical lines indicate the signal window used in the analysis. The dashed lines indicate the two sideband regions used for the background subtraction in each kinematic bin.

ZEUS

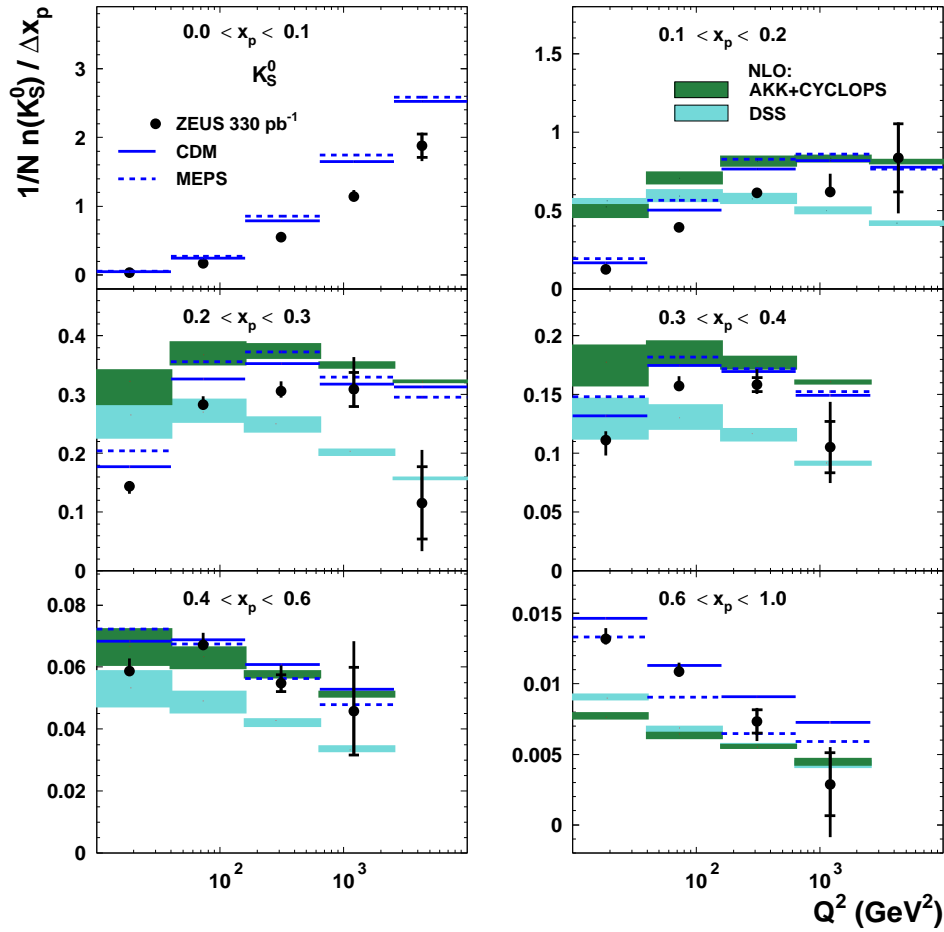


Figure 4: The measured scaled momentum distributions $(1/N)n(K_S^0)/\Delta x_p$ as functions of Q^2 in different regions of x_p (dots). The inner error bars represent the statistical uncertainty. The outer error bars show the statistical and systematic uncertainties added in quadrature. In some bins, the error bars on the data points are smaller than the marker size and are therefore not visible. For comparison, the NLO predictions of AKK+CYCLOPS (dark-shaded band) and DSS (light-shaded band) are also presented. The bands represent the theoretical uncertainty. The predictions from CDM (solid lines) and MEPS (dashed lines) are also shown.

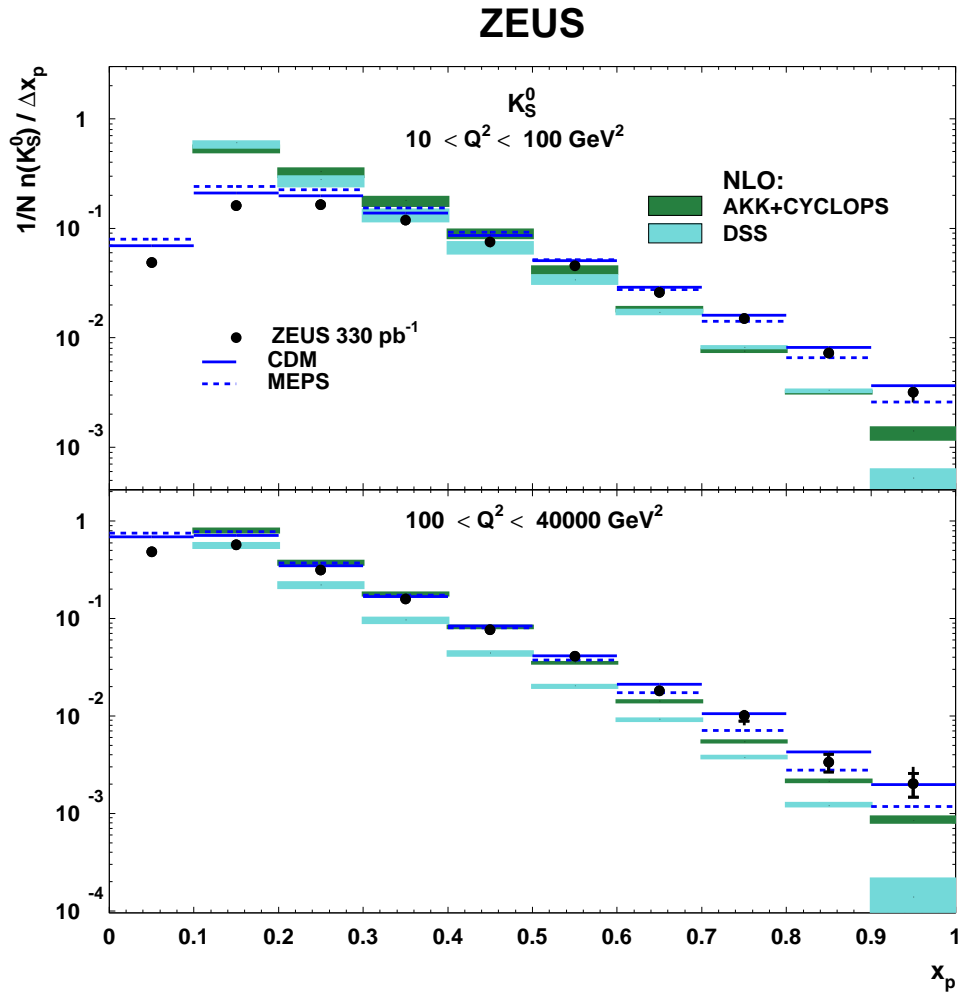


Figure 5: *The measured scaled momentum distributions $(1/N)(n(K_S^0)/\Delta x_p)$ as functions of x_p in different regions of Q^2 (dots). Other details as in the caption to Fig. 4.*

ZEUS

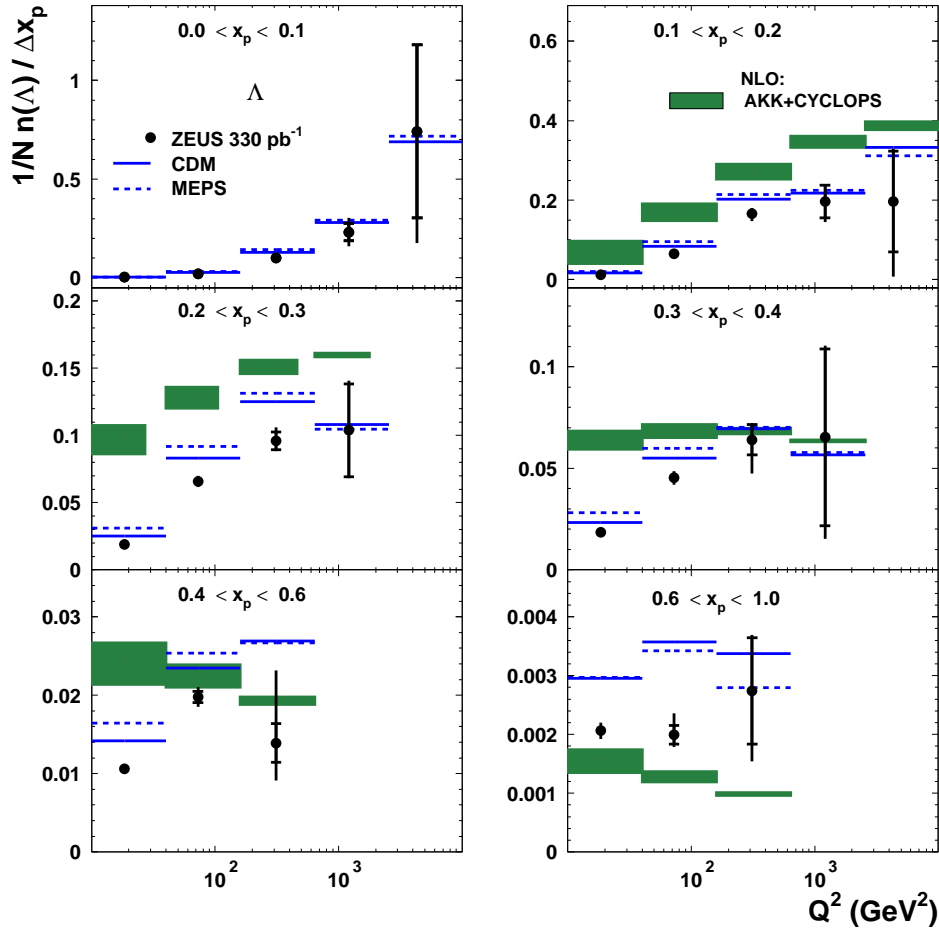


Figure 6: The measured scaled momentum distributions $(1/N)(n(\Lambda)/\Delta x_p)$ as functions of Q^2 in different regions of x_p (dots). Other details as in the caption to Fig. 4.

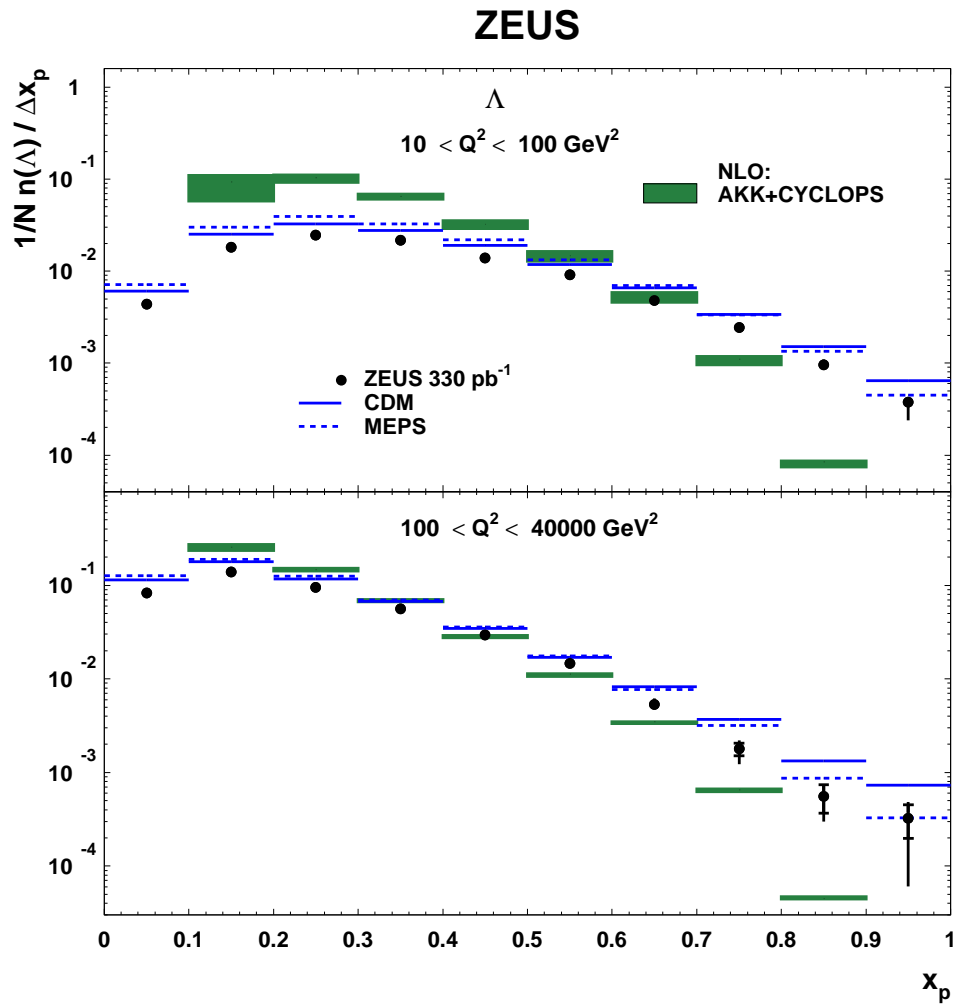


Figure 7: The measured scaled momentum distributions $(1/N)(n(\Lambda)/\Delta x_p)$ as functions of x_p in different regions of Q^2 (dots). Other details as in the caption to Fig. 4.

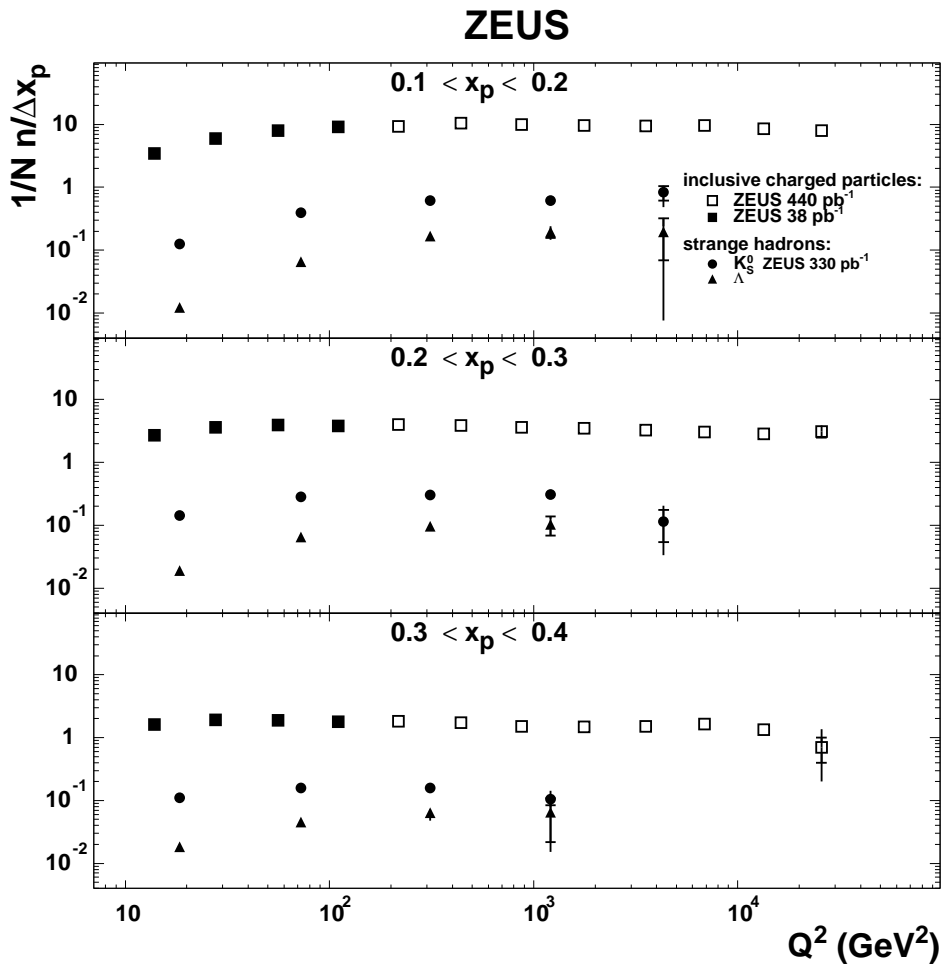


Figure 8: The measured scaled momentum distributions $(1/N)(n(H)/\Delta x_p)$ for $H = K_S^0$ (dots), Λ (triangles) and light charged particles (squares) as functions of Q^2 in different regions of x_p . Other details as in the caption to Fig. 4.